The final publication is available at Elsevier via https://dx.doi.org/10.1016/j.matdes.2018.04.046 © 2018. This manuscript version is made available under the CC-BY-NC-ND 4.0 license https://creativecommons.org/licenses/by-nc-nd/4.0/

Accepted Manuscript

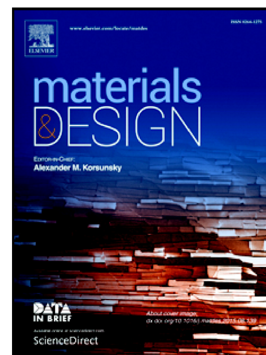

Bipolar resistive switching and memristive properties of hydrothermally synthesized TiO2 nanorod array: Effect of growth temperature

A.C. Khot, N.D. Desai, K.V. Khot, M.M. Salunkhe, M.A. Chougule, T.M. Bhave, R.K. Kamat, K.P. Musselman, T.D. Dongale

PII: S0264-1275(18)30316-2
DOI: doi:10.1016/j.matdes.2018.04.046
Reference: JMADE 3859

To appear in: *Materials & Design*

Received date: 9 February 2018
Revised date: 30 March 2018
Accepted date: 16 April 2018

Please cite this article as: A.C. Khot, N.D. Desai, K.V. Khot, M.M. Salunkhe, M.A. Chougule, T.M. Bhave, R.K. Kamat, K.P. Musselman, T.D. Dongale , Bipolar resistive switching and memristive properties of hydrothermally synthesized TiO2 nanorod array: Effect of growth temperature. The address for the corresponding author was captured as affiliation for all authors. Please check if appropriate. Jmade(2017), doi:10.1016/j.matdes.2018.04.046

This is a PDF file of an unedited manuscript that has been accepted for publication. As a service to our customers we are providing this early version of the manuscript. The manuscript will undergo copyediting, typesetting, and review of the resulting proof before it is published in its final form. Please note that during the production process errors may be discovered which could affect the content, and all legal disclaimers that apply to the journal pertain.

ACCEPTED MANUSCRIPT

Bipolar resistive switching and memristive properties of hydrothermally synthesized TiO_2 nanorod array: effect of growth temperature

A. C. Khot [a], N. D. Desai [b], K. V. Khot [c], M. M. Salunkhe [d], M. A. Chougule [e], T. M. Bhave [d], R. K. Kamat [f], K. P. Musselman [g], T. D. Dongale [a, $]

[a] Computational Electronics and Nanoscience Research Laboratory, School of Nanoscience and Biotechnology, Shivaji University, Kolhapur-416 004, India

[b] Department of Chemistry, Sanjay Ghodawat University, Kolhapur-416 118, India

[c] Department of General Engineering and Sciences, Sharad Institute of Technology, Ichalkaranji-416 115, India

[d] Department of Applied Physics, Defence Institute of Advanced Technology, Pune-411 025, India

[e] Department of Physics, Anandibai Raorane Arts, Commerce and Science College, Vaibhavwadi-416 810, India

[f] Department of Electronics, Shivaji University, Kolhapur-416 004, India

[g] Mechanical and Mechatronics Engineering, University of Waterloo, Waterloo, Ontario N2L 3G1, Canada

[$] **Corresponding Author's E-mail**: tdd.snst@unishivaji.ac.in (T. D. Dongale)

ACCEPTED MANUSCRIPT

ACCEPTED MANUSCRIPT

Abstract: In the present work, the hydrothermal approach is employed to develop 1D-TiO_2 nanorod array memristive devices and studied the effect of hydrothermal growth temperature on TiO_2 memristive devices. X-ray diffraction (XRD) analysis suggested that the rutile phase is dominant in the developed TiO_2 nanorod array. Field emission scanning electron microscopy (FESEM) images show well adherent and pinhole free one dimensional (1D) TiO_2 nanorods. The presence of titanium and oxygen in all the samples was confirmed by energy dispersive X-ray spectroscopy (EDS). Furthermore, growth of the 1D TiO_2 nanorods depends on the growth temperature and uniform growth is observed at the higher growth temperatures. The well-known memristive hysteresis loop is observed in the TiO_2 nanorod thin films. Furthermore, resistive switching voltages, the shape of I-V loops and (non)rectifying behavior changed as the growth temperature varied from 140 ^{o}C to 170 ^{o}C. The biological synapse properties such as paired-pulse facilitation and short-term depression are observed in some devices. The detailed electrical characterizations suggested that the developed devices show doubled valued charge-magnetic flux characteristic and charge transportation is due to the Ohmic and space charge limited current.

Keywords: Memristive device; TiO_2; Nanorods; Hydrothermal method; Resistive switching; Neuromorphic computing.

ACCEPTED MANUSCRIPT

ACCEPTED MANUSCRIPT

1. Introduction

In the era of big data analytics and artificial intelligence, extensive research in the field of new kinds of solid state memory devices and computing architectures is need of the hour. The conventional computer architecture shows the performance limitation due to the von Neumann bottleneck [1]. Along with the computer architecture, the basic building block of conventional memory and processing units are also not performing well in many areas such as footprint, speed and power consumption [2]. In order to achieve the future exascale computing capabilities, the basic building blocks of the conventional memory and processing unit need to be redefined. There are many possible solutions emerging in recent years to improve the performance metrics of computing systems. The brain-inspired neuromorphic computing architecture [3] and in-memory computing architecture [4-5] are two examples. Recently, the memristive device has emerged as a potential candidate to replace the flash-based memories [6-7] and also work as a basic building block for neuromorphic computing applications [8-9]. Furthermore, it can also be used for the in-memory computing architecture [10-11].

The memristor is popularly termed as the fourth fundamental circuit element along with the resistor, inductor and capacitor. It was theorized in 1971 by L. Chua [12] and experimentally demonstrated by HP lab in 2008, considering the dynamics of the oxygen vacancies as a state variable of a Pt/TiO_2/Pt nanodevice [13]. The experimental realization of memristor by HP lab is based on the resistive switching effect in Pt/TiO_2/Pt structure. The resistive switching effect in the metal-insulator-metal structure is well known to the scientific community, however, HP team took the brave step to correlate the resistive switching loop and memristor pinched hysteresis loop by the help of state variable 'w' [13]. On the other hand, the memristor reported by HP lab is not an ideal memristor but subclass memristive devices [14], as defined by Chua and Kang in 1976 [15]. In view of this, it is better to call TiO_2 resistive switch as a memristive device rather than memristor. In recent years, many materials were explored for the development of memristive devices after the landmark publication of the HP research group. These materials include, but are not limited to metal oxides [16], chalcogenides [17], polymers [18] and ferrites [19]. The metal oxides are a popular choice to develop the functional memristive devices. Among many metal oxide materials, TiO_2 is a potential material to fabricate two terminal memristive devices.

ACCEPTED MANUSCRIPT

This is due to fact that the TiO_2 based memristive device has a simple device structure, requires low power for operation, has good endurance and retention properties, and has CMOS compatibility [20].

The active layer of memristive devices can be developed using different physical deposition techniques. However, high processing cost and controlled environment make the physical deposition techniques unsuitable for the development of low-cost memristive and other electronic devices [21-26]. The literature survey reveals that the limited number of attempts were undertaken to develop a TiO_2 memristive device using low-cost solution processable techniques [27-31]. There have been many reports involving the use of nanorods in resistive switching devices, however, the effect of growth temperature was not studied systematically. In view of this, the present investigation deals with the development TiO_2 nanorod array memristive device using the low-cost hydrothermal method. In order to check the effect of growth temperature, the TiO_2 nanorod thin film memristive devices were developed at different growth temperatures such as 140, 150, 160 and 170 ^{o}C. The structural, morphological, and electrical characterizations were carried out in order to check the suitability of the developed devices for memory and computing application.

2. Experimental

2.1. Material and method

All chemicals used for the synthesis of a TiO_2 thin film were of analytical reagent grade and used without further purification. Here, a titanium isopropoxide (TTIP, $C_{12}H_{28}O_4Ti$, 98% spectrochem) was used as titanium precursor. In order to maintain the acidic condition of a reaction solution, concentrated hydrochloric acid (HCl, 36%, Thomas Baker) was used. The conducting fluorine doped tin oxide (FTO) was used as a starting substrate for the deposition of the TiO_2 thin film. The FTO substrates were cleaned ultrasonically with the help of ultrasonic bath sonicator and finally rinsed with the acetone. The crystal structure and phase identification were determined by X-ray diffraction (XRD) technique (Brucker AXS D8 model). The morphology and composition of all the deposited thin films were studied by field emission scanning electron microscopy (FESEM) equipped with energy dispersive X-ray spectroscopic (EDS) analyzer.

ACCEPTED MANUSCRIPT

2.2. Deposition of TiO_2 thin films

The TiO_2 thin films were deposited by using a single step hydrothermal method. In a typical synthesis of a TiO_2 thin film, 1:1 volume of double distilled water and concentrated HCl were taken. To this solution, 0.5 mL of TTIP solution was added and the solution was stirred for 30 min using a magnetic stirrer. The resulting clear and transparent solution was transferred into a Teflon lined autoclave with a 50 mL capacity. The FTO substrate was immersed in the reaction solution. The autoclave was sealed and placed in a hot air oven at 140 °C for 3 h. After cooling the autoclave to room temperature, the TiO_2 thin film was washed several times with deionized water. Furthermore, the developed films were annealed for 3 h at 350 °C in a hot air oven. The final film was abbreviated as T1. The above procedure was repeated for the 150, 160 and 170 °C and corresponding thin films were abbreviated as T2, T3, and T4 respectively. The preparative parameters for the deposition of TiO_2 thin films are given Table 1. In the present work, the reaction time was kept constant and temperature of the reaction bath (autoclave) was varied from 140 °C to 170 °C. The reaction temperature plays a key role in the growth mechanism of the TiO_2 thin film and the reaction temperature changes affect the thin film growth rate. In a typical synthesis of the TiO_2 thin film using the hydrothermal method, the high temperature and pressure were created using an autoclave. In view of this, the growth of TiO_2 thin film takes place by the process of heterogeneous nucleation [32-34]. In the present investigation, TTIP was used as a precursor of titanium and concentrated HCl was used to maintain the acidic conditions of reaction. The possible reaction occurs as follows, [35]

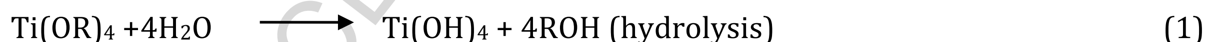

$Ti(OR)_4 + 4H_2O \longrightarrow Ti(OH)_4 + 4ROH$ (hydrolysis) (1)

$Ti(OH)_4 \longrightarrow TiO_2 + 2\,H_2O$ (condensation) (2)

2.3. Development of Ag/TiO_2/FTO thin film memristive device

The low-cost hydrothermal method was employed to synthesize TiO_2 thin films, which work as active layers in the memristive devices. The present memristive devices consist of three layers i.e. a top silver (Ag) layer, middle TiO_2 layer and bottom FTO layer. The Ag layer was patterned by vacuum deposition technique. All electrical measurements were carried out with the help of electrochemical workstation (Autolab N-Series). During all electrical measurements, the top Ag electrode was biased while bottom FTO electrode

ACCEPTED MANUSCRIPT

was grounded. The current-voltage (I-V) characteristic of developed devices was recorded by applying the appropriate SET and RESET voltages across the devices. Furthermore, the scan rate was increased from 100 mV/s to 500 mV/s in order to investigate the synaptic weight-like characteristics.

3. Result and Discussion

XRD was carried out in order to confirm the crystal structure of the deposited thin films. XRD measurements of developed thin films are shown in Fig. 1. The peaks observed in the XRD at 2Θ are 25.62°, 32.26°, 36.25°, 39.44°, 49.72°, 53.26°, 59.63° and 64.61° which are assigned to (110), (101), (200), (111), (211), (220), (002) and (310) planes respectively. XRD data are well matches with the rutile phase of the TiO2, which confirms the tetragonal crystal structure (JCPDS card no. 88-1175). XRD patterns exhibited strong diffraction peaks at 25.62°, 32.26° and 49.72° indicating TiO_2 in the rutile phase. The crystallite size (D) is calculated using the well-known Debye-Scherrer equation,

$$D = \frac{0.9\,\lambda}{\beta \cos \theta} \tag{3}$$

where D is crystallite size, λ represents the X-ray wavelength, β is the line broadening at full width half maximum and Θ represents the Bragg's angle. The calculated values for the crystallite size are 14.96 nm (T1), 21.65 nm (T2), 21.32 nm (T3) and 15.21 nm (T4) respectively. It is observed that the peak intensity of the diffraction pattern increases with increase in the crystallite size and peaks become wider for smaller crystallite size. The microstrain (ε) and dislocation density (δ) were calculated by the following equations,

$$\varepsilon = \frac{\beta \cos \theta}{4} \tag{4}$$

$$\delta = \frac{1}{\mathrm{D}^2} \tag{5}$$

The calculated values for the crystallite size, microstrain and dislocation density are summarized in Table 2. It is observed that the crystallite size becomes higher at moderate temperature (150 and 160 °C) and becomes lower at 140 and 170 °C. In addition, the microstrain and dislocation density parameters are found to be lower at moderate temperature and become higher for other temperatures. The morphology of the TiO_2 thin

ACCEPTED MANUSCRIPT

films is observed with the help of FESEM, as shown in Fig. 2. All FESEM images show the presence of well adherent, pinhole-free one dimensional (1D) TiO_2 nanorods. The FESEM images reveal that 1D TiO_2 nanorods uniformly cover the entire surface of the films. In the present work, the growth temperature is varied from 140 °C to 170 °C which results in the morphological transition. In the case of sample T1, the nanorods are not completely grown and they were oriented in random directions. As the temperature of the deposition increases, the TiO_2 nanorods show good growth and 1D nanostructure. The well-grown 1D TiO_2 nanorods provide a higher surface area than their compact thin film counterpart [36]. The electron mobility was calculated using the Mott–Gurney square law and it was found to be 8.32 x 10^{-6}, 5.25 x 10^{-5}, 1.30 x 10^{-4} and 3.88 x 10^{-5} $cm^2 V^{-1} s^{-1}$ for T1 to T4 devices, respectively. The well-grown 1D-TiO_2 nanorods devices (T3, T2) shows higher electron mobility than other devices. In view of this, well grown 1D nanorod structure provides excellent charge transport capability which is beneficial for the high-speed nanoelectronic devices [37-38]. The quantitative compositional analysis of T1, T2, T3 and T4 samples was carried out using EDS. The EDS spectra are shown in Fig. 3. The presence of titanium and oxygen in all the samples was confirmed by EDS. The observed atomic percentage of both the elements are in good agreement with an expected atomic percentage but not in the stoichiometric form. The non-stoichiometry of TiO_2 is may be due to tiny fluctuation in the hydrothermal and annealing conditions. The EDS spectra show two strong peaks at 4.50 and 0.52 keV for titanium and oxygen, respectively. The peaks observed at 4.50 and 5 keV are attributed to the Ti K_α and Ti K_β lines, respectively. It is observed that the oxygen content slightly decreases as the hydrothermal growth temperature increases from 140 ^oC to 170 ^oC. The decrease in the oxygen content is due to the out-diffusion of oxygen during the higher growth temperature [39]. There is no trace of any other impurities in the developed thin films within the detection limit of EDS.

The pinched hysteresis loop in the current-voltage (I-V) plane and nonlinear charge-magnetic flux (q-φ) relations are the basic criteria for the identification of the ideal memristor device. In many instances, the ideal memristor characteristics are not observed and these non-ideal devices are called extended memristor devices or memristive devices [40]. In Fig. 4, the I-V characteristics of Ag/TiO_2/FTO thin film devices developed using the hydrothermal technique at different growth temperatures (140 to 170 ^oC). The well-known

ACCEPTED MANUSCRIPT

hysteresis loop is clearly observed for all devices. This indicates that the developed devices behave like memristive devices. It is observed that the resistive switching voltages and shape of the I-V loops change as the growth temperature varied from 140 to 170 ^oC. In general, the active layer size increases as the growth temperature increases in the case of hydrothermally synthesized TiO_2 thin film [41] and, therefore, corresponding resistive switching voltages also increase [42-43]. Thus, the thicker active layer devices need to create sufficiently larger conductive filaments and, therefore, higher resistive switching voltages (V_{SET} and V_{RESET}) are required to create and break the conductive filament. On the other hand, lower resistive switching voltages can easily produce and rupture the conductive filament in the case of thin active layer memristive device. Furthermore, two distinct I-V hysteresis shapes are observed for the developed memristive devices. It is interesting to note that the T1 and T4 devices show the rectifying property or Schottky diode-like behavior. The rectifying behavior vanishes in the case of T2 and T3 devices. Furthermore, the area under lower loop (second quadrant) increases as the deposition temperature increases from 140 ^oC to 160^oC and decreases for the remaining case (170 ^oC). The observed rectifying behavior of Ag/TiO_2/FTO memristive devices may be due to the different concentration of oxygen vacancies which change the Schottky contact resistance at the Ag/TiO_2 interfaces and difference in the work function of the TiO_2 active layer and top Ag electrode [44-45]. In addition to this, the T1 and T4 devices show the non-stoichiometric atomic percentage of titanium and oxygen in the sample. It is observed that the atomic percentage of oxygen becomes higher for T1 device whereas it becomes lower for T4 device. Such kind of non-stoichiometry may be responsible for the rectifying I-V characteristics. It is interesting to note that the slight change in the oxygen percentage results in the different I-V characteristics. The dislocation density is an important factor in resistive switching which gives rise to pipe diffusion and modifies the local oxygen content through external stimulus [46]. In the present case, rectifying behavior is observed for higher dislocation density devices and non-rectifying behavior is observed for lower dislocation density devices. There is no correlation observed between dislocation density and current through the devices. These results suggest that the growth-temperature-dependent I-V characteristics of TiO_2 memristive devices can be useful for the development of reconfigurable nano-devices for memory and logic applications [47-48].

ACCEPTED MANUSCRIPT

To check the suitability of developed memristive devices for neuromorphic computing application, the scan rate is varied from 100 to 500 mV/s. The scan rate dependent I-V characteristics of the devices are shown in Fig. 5. The scan rate dependent study reveals that the current *i(t)* of the developed memristive devices can be modulated by varying the scan rate. In other words, the resistance of the devices can be changed by adopting scan rate variation strategy. Such kind of behaviour is important for the development of electronic synapse devices for neuromorphic computing applications. The aim of the electronic synapse is to mimic the functionality of a biological synapse. The biological synapse is a junction between a pre-synaptic neuron and a post-synaptic neuron and it is responsible for the learning as well as memory [1]. The learning and memory characteristics can be achieved by modulating the synaptic weights. The synaptic weight (SW) like behavior (maximum current *i(t)* at SET and RESET voltages) of Ag/TiO_2/FTO thin film memristive devices at positive and negative bias region is shown in Fig. 6 (a and b), respectively. The incremental SW like behaviour is observed for T1 device whereas T2 device shows decrease in the SWs in both bias regions. On the other hand, the strengths of the SWs are not improved for the T3 and T4 devices as the scan rate varied from 100 mV/s to 500 mV/s in the positive bias region. In the negative bias, T3 device does not show any improvement, however, the T4 device shows improvement in the SWs. The SW increase may be due to the local conductive filaments formation along with the original filament which results in increased local current density [49]. On the other hand, dissimilar oxygen vacancies density near the Ag/TiO_2 interface and stochastic formation and breaking of the conductive filament may be responsible for the decrease in the SWs in some devices. In the neurobiological terms, the improvements in the SWs are called paired-pulse facilitation and a decrease in the SWs are called short-term depression. The combined effect of facilitation and depression leads to the short-term synaptic plasticity [49]. In the present case, the T1 device shows the paired-pulse facilitation like characteristics while T2 device shows the short-term depression like characteristics. The short-term synaptic plasticity is similar to accumulator register found in the computing systems which store the intermediate results of arithmetic and logic operations. The short-term synaptic plasticity enhances the neural networks dynamics and provides new dimensions to the information processing. In view of

ACCEPTED MANUSCRIPT

this, the hydrothermally synthesized TiO_2 memristive device is a potential candidate for the development of electronic synapse for neuromorphic computing application.

The ideal memristor device is a two-terminal circuit element and it must show passivity in the I-V plane and nonlinearity in the charge and magnetic flux plane [12, 40]. The passivity corresponds to pinched hysteresis loop in I-V plane i.e. current should be zero at the origin (0V). The definition of an ideal memristor suggested that the q-φ characteristics should be always single-valued and nonlinear. However, practical devices possess double valued q-φ nonlinear characteristics [50-51]. The extended class of these devices is termed as memristive devices [40]. In order to check the devices developed in this work are either memristor or memristive, we have calculated the q-φ characteristic with the help of experimental time-dependent I-V characteristics. The following equations 6 and 7 are employed to calculate the q-φ characteristics [51]:

$$q(t) = \int_{-\infty}^{t} i(t)dt \quad (6)$$

$$\varphi(t) = \int_{-\infty}^{t} v(t)dt \quad (7)$$

The time domain charge, time domain magnetic flux and charge-magnetic flux behavior of T1 to T4 memristive devices are shown in Fig. 7 (a to c), respectively. The dotted arrow indicates the transition of the device from high resistance state (HRS) to low resistance state (LRS) and vice versa. The initial, half-period, final-period and turning points are labeled as A_1, B_{CW}, A_2, and B_{CW}^{N}, respectively. The CW represents the clockwise nature of the input stimulus.

The T3 memristive device shows the higher charge magnitude and T1 device shows the lower charge magnitude compared to other devices, as shown in Fig. 7 (a). This is due to fact that the T3 device possesses a higher hysteresis area and the T2 device has a lower hysteresis area than the other devices. It is interesting to note that every device shows the asymmetric time domain charge behavior i.e. initial charge values (A_1) and final charge values (A_2) are different. In other words, the oxygen vacancy distribution density may be changed after the resistive switching process completion. Furthermore, half-period points of all memristive devices are not identical which suggested that the hysteresis loop nature of all devices is different from each other. By looking at the time domain charge behavior,

ACCEPTED MANUSCRIPT

one can simply predict the symmetric and asymmetric nature of the hysteresis loop. Furthermore, the HRS/LRS ratio is termed the memory window and it can be correlated with the device reliability [52]. A higher memory window provides immunity to noise and leads to less read-write errors in the memory architecture. In the present case, the ratio of A_2 (HRS) and B_{CW} (LRS) can be termed as the memory window. In view of this, T2 and T3 devices show the higher memory window than other devices and they can be more reliable for memory applications. The time domain magnetic flux behavior of the devices is shown in Fig. 7 (b). It is observed that the developed devices show the symmetric time domain flux characteristics in the φ-t plane. This is due to fact that the symmetric SET and RESET voltages are applied to each device (only difference is the polarity). Furthermore, the magnitude of the flux increases as the growth temperature increases from 140 ^{o}C to 170 ^{o}C (T1 to T4 device). The increase in the flux is due to the increase in the resistive switching voltages (V_{SET} and V_{RESET}). From this result, one can conclude that the application of the symmetric resistive switching voltages leads to the symmetric φ-t characteristics and application of asymmetric resistive switching voltages results in the asymmetric φ-t characteristics. Furthermore, higher resistive switching voltages can create the higher magnetic flux magnitude. The charge-magnetic flux characteristic of T1 to T4 memristive devices is shown in Fig. 7 (c). Unlike the ideal memristor characteristics, the developed devices show the doubled valued charge-magnetic flux characteristic. This result further confirms that the developed devices are non-ideal memristor devices or memristive devices. The observed double valued charge-magnetic flux characteristic may be due to the asymmetric nature of the pinched hysteresis loop. The T2 device shows the quasi-symmetric I-V characteristics hence the charge-magnetic flux characteristic approaches a single-valued curve. On the other hand, other devices show highly asymmetric I-V hysteresis loops hence the double-valued charge-magnetic flux characteristic will be their intrinsic property. It is found that the turning points (B_{CW}^{N}) of the devices are dependent on the applied flux or resistive switching voltages and increases as the growth temperature increases from 140 ^{o}C to 170 ^{o}C (T1 to T4 device). The results suggest that the single-valued charge-magnetic flux characteristic can be obtained by symmetric I-V hysteresis loop.

ACCEPTED MANUSCRIPT

The conduction mechanisms of the memristive devices can be obtained by the plotting the I-V characteristics on a log-log scale and calculating slopes in the low and high voltage regions. Figs. 8 and 9 represents the double logarithmic I-V characteristics of the memristive devices in the positive and negative bias regions, respectively. In the low voltage region (0 to 0.1 V), the slopes of T1 and T2 devices are found to be ~1 for positive as well as negative biases. This indicates that the current is directly proportional to the applied voltage. In view of this, Ohmic conduction dominates in the low voltage region for both positive and negative biases for T1 and T2 memristive devices. The slopes of the T3 and T4 devices in the positive bias region (V < 0.1 V) are found to be very low. This indicates that the current of the devices increases very slowly during lower voltage range (V < 0.1 V) and follows non-Ohmic conduction mechanism. The shifting of the I-V crossing in the first quadrant proves the coexistence of memristive and parasitic memcapacitive behavior for the T3 and T4 devices, as shown in Fig. 8 [53]. In addition to this, the I-V crossing locations of T3 and T4 devices are shifted in the third quadrant which results in the coexistence of memristive and parasitic meminductive properties in the same device, as shown in Fig. 9 (c and d) [53]. However, the slopes of the T3 and T4 devices in the negative bias region are greater than in the positive bias region, which suggests that the parasitic meminductive property is lower than the parasitic memcapacitive property. Furthermore, the crossing locations of the T3 and T4 devices in the negative bias region are closer to zero than in the positive bias region. These results suggest that the quasi-Ohmic conduction mechanism is dominant in the negative bias region. The non-zero I-V crossing location suggests that the T3 and T4 devices are active memristive devices [54-55]. On the other hand, the exact zero I-V crossing suggests that the T1 and T2 devices are passive memristive devices [12]. In the high voltage region (V > 0.1 V), the slope magnitude is found to be greater than 1 for all devices. This suggests that the currents of all devices are abruptly increasing as a function of applied voltages. This behavior matches well with the space charge limited current (SCLC) model, when the device current is proportional to the square of applied voltage [56]. The above results suggest that the T1 and T2 devices can be termed as passive memristive devices, whereas T3 and T4 devices can be considered as active memristive devices. Furthermore, an Ohmic conduction mechanism is dominant in the low voltage region (V < 0.1 V) of parasitic element free memristive devices and a SCLC

ACCEPTED MANUSCRIPT

conduction mechanism dominates the high voltage region ($V > 0.1$ V). We are extending this work to develop the TiO_2 nanorod based electronic synapse device for neuromorphic computing application.

4. Conclusions

In conclusion, we have successfully developed TiO_2 memristive devices using a simple and cost-effective hydrothermal method and studied the effect of growth temperature on structural, morphological and electrical properties of the TiO_2 nanorod array memristive devices. XRD studies suggested that the rutile phase is dominant in the developed TiO_2 nanorod array (crystallite size ~ 14 nm to 22 nm). FESEM results suggested that the developed TiO_2 thin films possess a well adherent and pinhole free one dimensional (1D) nanorod structure. Furthermore, the 1D TiO_2 nanorods uniformly covered the entire surface and such kind of nanostructure provides a higher surface area with excellent charge transport capability. It is observed that the growth of the 1D TiO_2 nanorods depends on the growth temperature and uniform growth is observed at higher temperatures (160 °C and 170 °C). Bipolar resistive switching with the well-known memristive hysteresis loop is observed in the TiO_2 nanorod array. The resistive switching voltages, nature of I-V loops and (non)rectifying behavior are modified as a function of growth temperature. The results suggested that different concentration of oxygen vacancies at the Ag/TiO_2 interfaces and non-stoichiometric atomic percentage of titanium and oxygen results in the rectifying I-V characteristics. The scan rate variation studies suggest that the T1 and T2 devices can be used to develop an electronic synapse for mimicking the biological synapse characteristics such as paired-pulse facilitation and short-term depression, respectively. The detailed electrical characterizations suggested that the developed devices show doubled valued charge-magnetic flux characteristic and charge transportation is due to the Ohmic and space charge limited current.

ACCEPTED MANUSCRIPT

ACCEPTED MANUSCRIPT

Conflict of interest: The authors have no conflict of interest to disclose.

Author contributions: ACK, NDD, KVK, and TDD designed the experiment, synthesis the thin films and developed the devices. MMS, MAC and TMB characterize the devices. ACK, RKK, KPM, and TDD documented the manuscript. All authors reviewed the manuscript.

Acknowledgments: This work was supported by funding from School of Nanoscience and Biotechnology, Shivaji University, Kolhapur.

The raw data required to reproduce these findings are available to download from [INSERT PERMANENT WEB LINK(s)]. The processed data required to reproduce these findings are available to download from [INSERT PERMANENT WEB LINK(s)].

ACCEPTED MANUSCRIPT

ACCEPTED MANUSCRIPT

References

1. S. H. Jo, T. Chang, I. Ebong, B. B. Bhadviya, P. Mazumder, W. Lu, Nanoscale memristor device as synapse in neuromorphic systems. *Nano Letters*, *10*(4), 1297-1301, 2010.
2. M. J. Flynn, & P. Hung, Microprocessor design issues: thoughts on the road ahead. *IEEE Micro*, 25(3), 16-31,2005.
3. D. Monroe, Neuromorphic computing gets ready for the (really) big time. *Communications of the ACM*, 57(6), 13-15, 2014.
4. P. P. Chougule, B. Sen, T. D. Dongale, Realization of Processing In-memory Computing Architecture using Quantum Dot Cellular Automata, *Microprocessors and Microsystems*, 52, 49-58, 2017
5. P. P. Chougule, B. Sen, R. Mukherjee, P. S. Patil, R. K. Kamat, T. D. Dongale, Processing in Memory Realization Using Quantum Dot Cellular Automata (QCA): Proposal and Implementation, *Journal of Nano- and Electronic Physics*, 9(1), 01021-1-01021-5, 2017
6. P. F. Chiu, M. F. Chang, C. W. Wu, C. H. Chuang, S. S. Sheu, Y. S. Chen, & M. J. Tsai, Low store energy, low vddmin, 8T2R nonvolatile latch and sram with vertical-stacked resistive memory (memristor) devices for low power mobile applications. *IEEE Journal of Solid- Circuits State*, 47(6), 1483-1496, 2012.
7. T. D. Dongale, K. P. Patil, S. B. Mullani, K. V. More, S. D. Delekar, P. S. Patil, P. K. Gaikwad, and R. K. Kamat. Investigation of process parameter variation in the memristor based resistive random access memory (RRAM): Effect of device size variations. *Materials Science in Semiconductor Processing*, 35, 174-180, 2015.
8. G. Indiveri, B. Linares-Barranco, R. Legenstein G. Deligeorgis, & T. Prodromakis, Integration of nanoscale memristor synapses in neuromorphic computing architectures, *Nanotechnology*, 24(38), 384010, 2013.
9. T. D. Dongale, N. D. Desai, K. V. Khot, N. B. Mullani, P. S. Pawar, R. S. Tikke, V. B. Patil, P. P. Waifalkar, P. B. Patil, R. K. Kamat, P. S. Patil, P. N. Bhosale, Effect of surfactants on the data directionality and learning behaviour of Al/TiO_2/FTO thin film memristor-based electronic synapse, *Journal of Solid State Electrochemistry*, 21(9), 2753-2757, 2017.
10. Y. Levy, J. Bruck, Y. Cassuto, E. G. Friedman, A. Kolodny, E. Yaakobi, & S. Kvatinsky ,Logic operations in memory using a memristive Akers array. *Microelectronics Journal*, 45(11), 1429-1437, 2014.

ACCEPTED MANUSCRIPT

11. S. Kvatinsky, D. Belousov, S. Liman, G. Satat, N. Wald, E. G. Friedman, A. Kolodny, U. C. Weiser, MAGIC—Memristor-aided logic. *IEEE Transactions on Circuits and Systems II: Express Brief*s, 61(11),895-899, 2014.
12. L. Chua, Memristor-the missing circuit element. *IEEE Transactions on circuit theory*, 18(5), 507-519, 1971.
13. D. B. Strukov, G. S. Snider, D. R. Stewart, & R. S. Williams, The missing memristor found. *Nature*, 453(7191), 80-83, 2008.
14. S. Vongehr & X. Meng, The missing memristor has not been found. Scientific reports, 5, 11657, 2015.
15. L. O. Chua & S. M. Kang, Memristive devices and systems. Proceedings of the IEEE, 64(2), 209-223, 1976.
16. J. J. Yang, D. B. Strukov, & D. R. Stewart, Memristive devices for computing. *Nature Nanotechnology*, 8(1), 13-24, 2013.
17. Y. Li, Y. Zhong, L. Xu, J. Zhang, X. Xu, H. Sun & X. Miao, Ultrafast synaptic events in a chalcogenide memristor. *Scientific Reports*, 3, 1619, 2013.
18. T. Berzina, A. Smerieri, M. Bernabò, A. Pucci, G. Ruggeri, V. Erokhin, & M. P. Fontana, Optimization of an organic memristor as an adaptive memory element. *Journal of Applied Physics*, 105(12), 124515, 2009.
19. K. Cai, R. Wang, B. Li, & J. Zhou, Hysteretic current-voltage characteristic in polycrystalline ceramic ferrites. *Applied Physics Letters*, 97(12), 122501, 2010.
20. H. Y. Jeong, Y. I. Kim, J. Y. Lee, & S. Y. Choi, A low-temperature-grown TiO_2-based device for the flexible stacked RRAM application. *Nanotechnology*, 21(11), 115203, 2010.
21. K. H. Choi, M. Mustafa, K. Rahman, B. K. Jeong, and Y. H. Doh, Cost-effective fabrication of memristive devices with ZnO thin film using printed electronics technologies, *Appl. Phys. A* 106(1), 165-170, 2012.
22. C. V. Ramana, S. Utsunomiya, R. C. Ewing, U. Becker, V. V. Atuchin, V. S. Aliev, V. N. Kruchinin, Spectroscopic ellipsometry characterization of the optical properties and thermal stability of ZrO2 films made by ion-beam assisted deposition. Applied Physics Letters, 92(1), 011917, 2008.
23. V. A. Shvets, V. S. Aliev, D. V. Gritsenko, S. S. Shaimeev, E. V. Fedosenko, S. V. Rykhlitski, V. V. Atuchin, V. A. Gritsenko, V. M. Tapilin, and H. Wong, Electronic structure and

ACCEPTED MANUSCRIPT

charge transport properties of amorphous Ta2O5 films, Journal of Non-Crystalline Solids, 354 (26), 3025-3033, 2008.

24. C. V. Ramana, R. S. Vemuri, V. V. Kaichev, V. A. Kochubey, A. A. Saraev, and V. V. Atuchin, X-ray photoelectron spectroscopy depth profiling of La2O3/Si thin films deposited by reactive magnetron sputtering, ACS applied materials & interfaces, 3 (11), 4370-4373, 2011.
25. V. H. Mudavakkat, V. V. Atuchin, V. N. Kruchinin, A. Kayani, C. V. Ramana, Structure, morphology and optical properties of nanocrystalline yttrium oxide (Y2O3) thin films. Optical Materials, 34(5), 893-900, 2012.
26. V. M. Kalygina, I. S. Egorova, I. A. Prudaev, O. P. Tolbanov, V. V. Atuchin, Photoelectrical characteristics of TiO2-N-SI heterostructures. Microwave and Optical Technology Letters, 58(5), 1113-1116, 2016.
27. V. Prusakova, C. Armellini, A. Carpentiero, A. Chiappini, C. Collini, S. Dirè, M. Ferrari, L. Lorenzelli, M. Nardello, S. Normani, A. Vaccari. Morphologic, structural, and optical characterization of sol-gel derived TiO_2 thin films for memristive devices. *Physica Status Solidi (c)*,12(1-2), 192-198, 2015
28. T. D. Dongale, S. S. Shinde, R. K. Kamat, & K. Y. Rajpure, Nanostructured TiO_2 thin film memristor using hydrothermal process. *Journal of Alloys and Compounds*, 593, 267-270, 2014.
29. H. Abunahla, M. A. Jaoude C. J. O'Kelly, & B. Mohammad, Sol-gel/drop-coated micro-thick TiO_2 memristors for g-ray sensing. *Materials Chemistry and Physics*, 184, 72-81, 2016.
30. N. Duraisamy, N. Muhammad, H. Kim, J. Jo, K. Choi, Fabrication of TiO_2 thin film memristor device using electrohydrodynamic inkjet printing. *Thin Solid Films*, 520(15), 5070-5074, 2012.
31. N. Gergel-Hackett, B. Hamadani, B. Dunlap, J. Suehle, C. Richter, C. Hacker, D. Gundlach, A flexible solution-processed memristor, *IEEE Electron Device Letters*, 30(7), 706-708, 2009.
32. K. Kakiuchi, E. Hosono, H. Imai, T. Kimura, and S. Fujihara, {111}-faceting of low-temperature processed rutile TiO_2 rods, *Journal of Crystal Growth*, 293(2), 541-545, 2006.

ACCEPTED MANUSCRIPT

ACCEPTED MANUSCRIPT

33. Y. Zhao, X. Gu & Y. Qiang, Influence of growth time and annealing on rutile TiO2 single-crystal nanorod arrays synthesized by hydrothermal method in dye-sensitized solar cells. Thin Solid Films, 520(7), 2814-2818, 2012.
34. S. Zhang, X. Gu, Y. Zhao, Y. Qiang, Enhanced Photoelectrochemical Performance of TiO 2 Nanorod Arrays by a 500° C Annealing in Air: Insights into the Mechanism. Journal of Electronic Materials, 45(1), 648-653, 2016.
35. D. B. Shinde, S. K. Jagadale, R. K. Mane, R. M. Mane, V. B. Ghanwat, K. V. Khot, S. S. Mali C. K. Hong, P. N. Bhosale, Time Dependent Facile Hydrothermal Synthesis of TiO_2 Nanorods and their Photoelectrochemical Applications. *Journal of Nanomedicine & Nanotechnology*, S7 (4), 1-7, 2015
36. B. Liu, and S. E. Aydil, Growth of oriented single-crystalline rutile TiO_2 nanorods on transparent conducting substrates for dye-sensitized solar cells, *Journal of the American Chemical Society* 131, 3985-3990, 2009.
37. H. Zhang, X. Liu, Y. Li, Q. Sun, Y. Wang, B.J. Wood, P. Liu, D. Yang, and H. Zhao, Vertically aligned nanorod-like rutile TiO_2 single crystal nanowire bundles with superior electron transport and photoelectrocatalytic properties. *Journal of Materials Chemistry*, 22(6), 2465-2472, 2012.
38. R.S. Chen, C.A. Chen, H.Y. Tsai, W.C. Wang, and Y.S. Huang,. Photoconduction properties in single-crystalline titanium dioxide nanorods with ultrahigh normalized gain. *The Journal of Physical Chemistry* C, 116(6), 4267-4272, 2012.
39. A. N. H. Al-Ajili and S. C. Bayliss, A study of the optical, electrical and structural properties of reactively sputtered InOx and ITOx thin films. Thin Solid Films, 305(1-2), 116-123, 1997.
40. Y. V. Pershin, & M. D. Ventra, Memory effects in complex materials and nanoscale systems. *Advances in Physics,* 60(2), 145-227, 2011.
41. Y. Li, M. Zhang, M. Guo, and X. Wang, Hydrothermal growth of well-aligned TiO_2 nanorod arrays: Dependence of morphology upon hydrothermal reaction conditions. *Rare Metals*, 29(3), 286-291. 2010.
42. T. D. Dongale, S. V. Mohite, A. A. Bagade, R. K. Kamat, K. Y. Rajpure, Bio-mimicking the synaptic weights, analog memory, and forgetting effect using spray deposited WO_3 memristor device, *Microelectronic Engineering*, 183-184, 12-18, 2017.

ACCEPTED MANUSCRIPT

43. P. S. Pawar, R. S. Tikke, V. B. Patil, N. B. Mullani, P. P. Waifalkar, K. V. Khot, A. M. Teli, A. D. Sheikh, T. D. Dongale, A low-cost copper oxide thin film memristive device based on successive ionic layer adsorption and reaction method, *Material Science in Semiconductor Processing*, 71, 102–108, 2017.
44. T. Bertaud, M. Sowinska, D. Walczyk, S. Thiess, A. Gloskovskii, C. Walczyk, and T. Schroeder, In-operando and non-destructive analysis of the resistive switching in the Ti/HfO_2/TiN-based system by hard x-ray photoelectron spectroscopy. *Applied Physics Letters*, 101(14), 143501, 2012.
45. B. Long, J. Ordosgoitti, R. Jha, and C. Melkonian, Understanding the charge transport mechanism in VRS and BRS states of transition metal oxide nanoelectronic memristor devices. *IEEE Transactions on Electron Devices*, 58(11), 3912-3919, 2011.
46. K. Szot, W. Speier, G. Bihlmayer, R. Waser, Switching the electrical resistance of individual dislocations in single-crystalline SrTiO3. Nature materials, 5(4), 312, 2006.
47. T. D. Dongale, A. A. Bagade, S. V. Mohite, A. D. Rananavare, M. K. Orlowski, R. K. Kamat, K. Y. Rajpure, Bipolar resistive switching with coexistence of mem-elements in the spray deposited $CoFe_2O_4$ thin film, *Journal of Materials Science: Materials in Electronics*, 10.1007/s10854-017-8258-7.
48. T. D. Dongale, N. D. Desai, K. V. Khot, C. K. Volos, P. N. Bhosale, R. K. Kamat, An electronic synapse device based on TiO2 thin film memristor, Journal of Nanoelectronics and Optoelectronics, 13 (3), 68–75, 2018.
49. S.G. Hu, Y. Liu, T.P. Chen, Z. Liu, Q. Yu, L.J. Deng, Y. Yin, and S. Hosaka, Emulating the paired-pulse facilitation of a biological synapse with a NiOx-based memristor. *Applied Physics Letters*, 102(18), 183510, 2013.
50. N. Du, Y. Shuai, W. Luo, C. Mayr, R. Schüffny, O. G. Schmidt, and H. Schmidt, Practical guide for validated memristance measurements. *Review of Scientific Instruments*, 84(2), 023903, 2013.
51. Y. Shuai, N. Du, X. Ou, W. Luo, S. Zhou, O.G. Schmidt, and H. Schmidt, Improved retention of nonvolatile bipolar $BiFeO_3$ resistive memories validated by memristance measurements. *Physica Status Solidi (c),* 10(4), 636-639, 2013.
52. T. D. Dongale, K. V. Khot, S. V. Mohite, N. K. Desai, S. S. Shinde, V. L. Patil, S. A. Vanalkar, A. V. Moholkar, K. Y. Rajpure, P. N. Bhosale, P. S. Patil, P. K. Gaikwad, R. K. Kamat, Effect

of write voltage and frequency on the reliability aspects of Memristor-based RRAM, *International Nano Letters*, 7(3), 209-216, 2017.

53. L. Qingjiang, A. Khiat, I. Salaoru, C. Papavassiliou, X. Hui, T. Prodromakis, *Scientific Reports,* 4, 1–6, 2014.
54. S. Tappertzhofen, E. Linn, U. Bottger, R. Waser, and I. Valov, Nanobattery effect in RRAMs—implications on device stability and endurance. *IEEE Electron Device Letters*, 35(2), 208-210. 2014.
55. I. Valov, E. Linn, S. Tappertzhofen, S. Schmelzer, J. Van den Hurk, F. Lentz, and R. Waser, Nanobatteries in redox-based resistive switches require extension of memristor theory. *Nature Communications*, 4, 1771, 2013.
56. T. D. Dongale, K. P. Patil, P. K. Gaikwad, R. K. Kamat, Investigating Conduction Mechanism and Frequency Dependency of Nanostructured Memristor Device, *Materials Science in Semiconductor Processing*, 38, 228–233, 2015.

ACCEPTED MANUSCRIPT

ACCEPTED MANUSCRIPT

Table 1: Preparative parameters for the deposition of TiO_2 thin films

Sample Code	Bath Composition	Deposition Temperature (°C)	Time (hours)
T1	0.5 mL TTIP+ equal Volume of D/w and Conc. HCl	140	3
T2		150	
T3		160	
T4		170	

ACCEPTED MANUSCRIPT

ACCEPTED MANUSCRIPT

Table 2: Crystallite size, microstrain and dislocation density of TiO_2 thin films

Sample Code	Crystallite Size (nm)	Microstrain X 10^{-3} (line^{-2} m^{-4})	Dislocation Density X 10^{-3} (nm^{-2})
T1	14.96	2.315	4.46
T2	21.65	1.608	2.13
T3	21.32	1.609	2.20
T4	15.21	2.240	4.32

ACCEPTED MANUSCRIPT

ACCEPTED MANUSCRIPT

Fig. 1: XRD pattern of (a) T1, (b) T2, (c) T3 and (d) T4 TiO_2 thin films, developed at different deposition temperature (140 ^oC to 170 ^oC with step size 10 ^oC, respectively)

Fig. 2: Low and high magnification FESEM images of (a) T1, (b) T2, (c) T3, and (d) T4 TiO_2 thin films.

Fig. 3: EDS spectra of (a) T1, (b) T2, (c) T3, and (d) T4 TiO_2 thin films. Inset shown in all figures represent the atomic percentage of Titanium (Ti) and Oxygen (O).

Fig. 4: I-V characteristics of Ag/TiO_2/FTO thin film memristive devices developed at (a) 140 ^oC, (b) 150 ^oC, (c) 160 ^oC, and (d) 170 ^oC hydrothermal deposition temperature. The deposition temperature dependent hysteresis loop is clearly observed in the memristive devices. The direction of resistive switching is indicated by the arrows and insets represented the Schottky diode-like behavior.

Fig. 5: Scan rate dependent I-V characteristics of (a) T1, (b) T2, (c) T3, and (d) T4 thin film memristive devices. The scan rate is varied from 100 mV/s to 500 mV/s to investigate the possible synaptic weight like behavior.

Fig. 6: Synaptic weight (SW) like the behavior of Ag/TiO_2/FTO thin film memristive devices at (a) positive and (b) negative bias.

Fig. 7: (a) Time domain charge, (b) Time domain magnetic flux and (c) Charge-magnetic flux behavior of T1 to T4 memristive devices. The dotted arrows represent the HRS to LRS and LRS to HRS transition.

Fig. 8: Double logarithmic I-V characteristics of (a) T1, (b) T2, (c) T3, and (d) T4 devices in positive bias region. The inset represents the parasitic memcapacitive property coexisted with the memristive property.

Fig. 9: Double logarithmic I-V characteristics of (a) T1, (b) T2, (c) T3, and (d) T4 devices in negative bias region. The inset represents the parasitic meminductive property coexisted with the memristive property.

ACCEPTED MANUSCRIPT

ACCEPTED MANUSCRIPT

Highlights

- Developed well adherent and pinhole free one dimensional (1D) Rutile-TiO_2 nanorod array and studied the growth temperature dependent memristive properties

- Bipolar resistive switching with well known memristive hysteresis loop is observed in the TiO_2 nanorod array

- Resistive switching voltages, shape of I-V loops and (non)rectifying behavior are depends upon the growth temperature

- Paired-pulse facilitation and short-term depression like characteristics are observed

- Non-ideal doubled valued charge-magnetic flux characteristic is observed

- Conduction mechanism is due to Ohmic and space charge limited current

ACCEPTED MANUSCRIPT